SLAC-PUB-12152
astro-ph/0610181
October 2006

Evidence for the importance of resonance scattering in X-ray emission line profiles of the O star ζ Puppis

Maurice A. Leutenegger[1], Stanley P. Owocki[2], Steven M. Kahn[3], Frits B. S. Paerels[1]

ABSTRACT

We fit the Doppler profiles of the He-like triplet complexes of O VII and N VI in the X-ray spectrum of the O star ζ Pup, using XMM-*Newton* RGS data collected over $\sim$ 400 ks of exposure. We find that they cannot be well fit if the resonance and intercombination lines are constrained to have the same profile shape. However, a significantly better fit is achieved with a model incorporating the effects of resonance scattering, which causes the resonance line to become more symmetric than the intercombination line for a given characteristic continuum optical depth τ_*. We discuss the plausibility of this hypothesis, as well as its significance for our understanding of Doppler profiles of X-ray emission lines in O stars.

Subject headings: stars: early type — star: winds, outflows — techniques: spectroscopic — stars: individual (ζ Pup)

1. Introduction

High resolution X-ray spectra obtained with diffraction grating spectrometers on the *Chandra* and XMM-*Newton* X-ray observatories have revolutionized our understanding of the X-ray emission of O stars in the last five years. In the canonical picture, the X-rays are emitted in plasmas heated by shocks distributed throughout the wind (Cassinelli & Swank 1983; Corcoran et al. 1993; Hillier et al. 1993; Corcoran et al. 1994); the shocks are created

[1]Department of Physics and Columbia Astrophysics Laboratory, Columbia University, 550 West 120th Street, New York, NY 10027;

maurice@astro.columbia.edu

[2]Bartol Research Institute, University of Delaware, 217 Sharp Laboratory, Newark, DE 19716

[3]Kavli Institute for Particle Astrophysics and Cosmology, Stanford Linear Accelerator Center and Stanford University, 2575 Sand Hill Road, Menlo Park, CA 94025

Submitted to Astrophys.

Work supported in part by Department of Energy contract DE-AC02-76SF00515

by instabilities in the radiative driving force (e.g. Lucy & White 1980; Owocki, Castor, & Rybicki 1988; Cooper 1994; Feldmeier, Puls, & Pauldrach 1997). Although some stars show anomalous X-ray emission that can be explained by a hybrid mechanism involving winds channelled by magnetic fields (e.g. τ Sco and θ^1 Ori C, Donati et al. 2002; Cohen et al. 2003; Gagné et al. 2005; Donati et al. 2006), a number of "normal" O stars have X-ray spectra that are mostly consistent with the wind-shock paradigm (e.g. ζ Pup, ζ Ori, δ Ori). The works describing the first few high resolution spectra of normal O stars obtained found some inconsistencies with expectations (Waldron & Cassinelli 2001; Kahn et al. 2001; Cassinelli et al. 2001; Miller et al. 2002; Waldron et al. 2004), but more recent quantitative work based on the simple empirical Doppler profile model of Owocki & Cohen (2001, hereafter OC01) has resolved many of these problems (Kramer, Cohen, & Owocki 2003; Cohen et al. 2006; Leutenegger et al. 2006). The main outstanding problem is the relative lack of asymmetry in emission line Doppler profiles, which, if taken at face value, would imply reductions in the literature mass-loss rates of an order of magnitude (Kramer et al. 2003; Cohen et al. 2006; Owocki & Cohen 2006).

Although there is mounting evidence from other lines of inquiry suggesting that the literature mass-loss rates may be systematically too high (Massa et al. 2003; Hillier et al. 2003; Bouret, Lanz, & Hillier 2005; Fullerton, Massa, & Prinja 2006), there are also subtle radiative transfer effects that could cause emission line profiles to be more symmetric than one might naively expect. Two effects that have been investigated in the literature are porosity (Feldmeier, Oskinova, & Hamann 2003; Oskinova, Feldmeier, & Hamann 2004, 2006; Owocki & Cohen 2006) and resonance scattering (Ignace & Gayley 2002, hereafter IG02). Porosity could lower the effective opacity of the wind to X-rays, thus symmetrizing emission lines. However, Oskinova et al. (2006) and Owocki & Cohen (2006) have found that the characteristic separation scale of clumps must be very large to show an appreciable effect on line profile shapes, which makes it difficult to achieve a significant porosity effect. Resonance scattering can symmetrize Doppler profiles by favoring lateral over radial escape of photons; it is an intriguing possibility, but to date it has not been tested experimentally.

In this paper, we present evidence for the importance of resonance scattering in some of the X-ray emission lines in the spectrum of the O star ζ Pup. We show that the blend of resonance and intercombination lines of two helium-like triplets in the very high signal-to-noise XMM Reflection Grating Spectrometer (RGS) spectrum of ζ Pup cannot be well fit assuming that both lines have the same profile, but can be much better fit assuming the profile of the resonance line is symmetrized by resonance scattering.

This paper is organized as follows: in § 2 we discuss the reduction of over 400 ks of XMM RGS exposure on ζ Pup; in § 3 we briefly recapitulate the results of OC01 and Leutenegger

et al. (2006) for Doppler profile modelling (§ 3.1), and we show that the He-like OC01 profile model does not give a good fit to the O VII and N VI triplets of ζ Pup (§ 3.2); in § 4 we generalize the results of OC01 to include the effects of resonance scattering as derived in IG02 (§ 4.1), and we fit this model to the data (§ 4.2); in § 5 we discuss our results; and in § 6 we give our conclusions.

2. Data reduction

The data were acquired in eleven separate pointings. The first two observations were Performance Verification, while the rest were Calibration; they are all available in the public archive. The ODFs were processed with SAS 7.0.0 using standard procedures; periods of high background were filtered out. Only RGS (den Herder et al. 2001) data were used in this paper, but EPIC data are available for most of the observations. Processing resulted in a coadded total of 415 ks of exposure in RGS 1 and 412 ks in RGS 2. The observation IDs used and net exposure times are given in Table 1.

RGS has random systematic wavelength scale errors with a 1σ value of ± 7 mÅ (den Herder et al. 2001). A 7 mÅ shift could lead to significant systematic errors in the model parameters measured from a line profile. Because of this, we coadd all observations using the SAS task `rgscombine`. Assuming the systematic shifts are randomly distributed, coadding the data will result in a spectrum that is almost unshifted (depending on the particular distribution of shifts of the individual observations), but that is broadened by 7 mÅ; this effect is much easier to account for in our analysis. We have assumed that the data do not vary intrinsically. We have not formally verified that the data show no significant intrinsic variation, but upon visual inspection the data do not appear to vary more than expected from statistical fluctuations combined with the aforementioned random systematic errors in the wavelength scale.

Spectral fitting was done with XSPEC 12.2.1; the line profile models are implemented as local models. The C statistic (Cash 1979) is used instead of χ^2 because of the low number of counts per bin in the wings of the profiles.

Because of the failed CCD on RGS2, we only have RGS1 data for O VII He α. We only fit RGS2 data for N VI He α because the complex falls on a chip gap for RGS1.

For each complex we fit, we first measured a local continuum strength from a nearby part of the spectrum uncontaminated by spectral features. We modeled this continuum as a power-law with an index of two, which is flat when plotted against wavelength. When fitting a line profile, we fit a combination of the local continuum (fixed to the measured value) plus

the line profile model to the data.

For the N VI He α complex, we also included emission from C VI Lyman β at 28.4656 Å, since the red wing of this line overlaps the blue wing of the resonance line of N VI He α. The model parameters for C VI Lyman β are assumed to be the same as for N VI, and it is assumed to be optically thin to resonance scattering.

Emission lines and complexes were fit over a wavelength range of $\lambda_- < \lambda < \lambda_+$. Here $\lambda_\pm = \lambda_0(1 \pm v_\infty/c) \pm \Delta\lambda$, where $\Delta\lambda$ is the resolution of RGS at that wavelength. λ_0 is the shortest wavelength in the complex for λ_- and the longest wavelength for λ_+.

3. Best fit He-like profile model

3.1. The profile model

In this section we briefly recapitulate the results of OC01 for the Doppler profile of an X-ray emission line from an O-star wind, and the extension of these results to a He-like triplet complex by Leutenegger et al. (2006).

In the physical picture of the OC01 model, the wind is a two-component fluid; the bulk of the wind is relatively cool material of order the photospheric temperature, while a small fraction of the wind is at temperatures of order 1-5 MK, so that it emits X-rays. The cool part of the wind has some continuum opacity to X-rays and can absorb them as they leave the wind.

The OC01 formalism casts the line profile in terms of a volume integral over the emissivity, attenuated by continuum absorption:

$$L_\lambda = 4\pi \int dV \eta_\lambda(\mu, r) e^{-\tau(\mu,r)} \tag{1}$$

where $\eta_\lambda(\mu, r)$ is the emissivity at the observed wavelength λ and $\tau(\mu, r)$ is the continuum optical depth to X-rays of the wind.

The line profile can be expressed in terms of the scaled wavelength $x \equiv (\lambda/\lambda_0 - 1)c/v_\infty = -v_z/v_\infty$; this gives the shift from line center in the observer's frame in units of the wind terminal velocity. The sign convention is such that positive x corresponds to a redshift.

OC01 derive an expression for the line profile in terms of an integral over the inverse radial coordinate $u = R_*/r$:

$$L_x = L_0 \int_0^{u_x} du \, \frac{f_X(u)}{w^3(u)} e^{-\tau(x,u)}. \tag{2}$$

In this equation we have used the following expressions: $w(u) \equiv v(u)/v_\infty = (1-u)^{\beta_v}$ is the scaled velocity; $\tau(x,u)$ is the (continuum) optical depth to X-rays emitted along a ray to the observer; $f_X(u) \propto u^q$ is the filling factor of X-ray emitting plasma; and $u_x \equiv \min(u_0, 1-|x|^{1/\beta_v})$ is the upper limit to the integral. $u_0 = R_*/R_0$ is the inverse of the minimum radius of X-ray emission R_0, and $1-|x|^{1/\beta_v}$ is a geometrical cutoff for the minimum radius that emits for a given value of x. We have used β_v as the exponent of the velocity law rather than the customary β to avoid confusion later in the paper. The integral for L_x can be evaluated numerically.

The optical depth in this expression is derived in OC01. It is written as the product of the characteristic optical depth $\tau_* = \kappa\dot{M}/4\pi R_* v_\infty$ times a dimensionless integral containing only terms depending on the geometry. It can be evaluated analytically for integer values of β_v. For non-integer values of β_v, the optical depth must be evaluated numerically, which is computationally costly, and thus not convenient in conjunction with the radial integral of the line profile. Because of this we assume $\beta_v = 1$ throughout this paper, which is a good approximation for ζ Pup, and also for O stars in general.

The interesting free parameters of this model are the exponent of the radial dependence of the X-ray filling factor, q; the characteristic optical depth to X-rays of the cold plasma, τ_*; and the minimum radius for the onset of X-ray emission R_0.

Leutenegger et al. (2006) extend this analysis to a He-like triplet complex. The only difference is that the forbidden-to-intercombination line ratio has a radial dependence due to photoexcitation of the metastable upper level of the forbidden line:

$$\mathcal{R} \equiv \frac{f}{i} = \mathcal{R}_0 \frac{1}{1+\phi/\phi_c} = \mathcal{R}_0 \frac{1}{1+2PW(r)}. \tag{3}$$

Here ϕ is the photoexcitation rate from the upper level of the forbidden line; it depends on the photospheric UV flux and scales with the geometrical dilution $W(r)$; ϕ_* is the photoexcitation rate near the photosphere, so that $\phi = 2\phi_* W(r)$; ϕ_c is the critical photoexcitation rate, which is a parameter of the ion; and $P = \phi_*/\phi_c$ is a convenient dimensionless parameter that gives the relative strength of photoexcitation and decay to ground near the star such that $\mathcal{R}(R_*) = \mathcal{R}_0/(1+P)$. In this paper, we use values of P calculated from TLUSTY stellar atmosphere models (Lanz & Hubeny 2003) as described in Leutenegger et al. (2006). Values of $\mathcal{R}_0$ are taken from Porquet et al. (2001).

To modify the expressions for the forbidden and intercombination line profiles to account for this effect, the emissivity is multiplied by the normalized line ratio:

$$\eta_f(r) = \eta(r) \frac{\mathcal{R}(r)}{1+\mathcal{R}(r)} \tag{4}$$

and

$$\eta_i(r) = \eta(r)\frac{1}{1+\mathcal{R}(r)}. \quad (5)$$

3.2. Best fit model

In this section we model the Doppler profiles of the O VII and N VI He-like triplets with the He-like profile of Leutenegger et al. (2006) described in § 3.1. The forbidden line is very weak for these two ions, and the intercombination line profile predicted by the model is not very different from the resonance line profile. The main difference in the profile of the resonance and intercombination lines is that the extremes of the wings are somewhat weaker. This is because the f/i ratio reverts to the low-UV-flux limit at very large radii ($> 100R_*$ for O VIII for ζ Pup), so that the intercombination line strength is reduced by a factor of a few. However, this has only a small effect on the profile shape.

Although it is weak, the predicted strength of the forbidden line is a good check on the consistency of the profile model. The value of the characteristic optical depth τ_* can have a strong effect on the observed f/i ratio by setting the value of R_1, the radius of optical depth unity. However, this effect is degenerate with the value of q, the exponent of the radial dependence of the X-ray filling factor.

In Figures 1 and 2, we show the Doppler profiles of the O VII and N VI He-like triplets, together with the best fit models. The best-fit parameters are given in Table 2 and 3. There are significant residuals in both fits. The N VI triplet shows stronger residuals than O VII. The residuals have a systematic shape: the model predicts a greater flux than the data on the blue wing of the resonance line and the red wing of the intercombination line, while it underpredicts the data in the center of the blend.

The systematic nature of the residuals implies that there is something different about the shapes of the Doppler profiles of the resonance and intercombination lines. Qualitatively, the residuals are consistent with the model resonance line being too blue and therefore too asymmetric, and the model intercombination line being too red and therefore too symmetric.

Resonance scattering has been proposed by IG02 as an explanation for the properties of O-star X-ray emission line Doppler profiles. If it is important, it can cause significant symmetrization of profiles of strong resonance lines. Because this is in qualitative agreement with our observations, we explore this idea further.

4. Best fit model including the effects of resonance scattering

4.1. Incorporating resonance scattering into OC01

In this section we discuss the modifications to the model of OC01 needed to include the effects of resonance scattering. The calculation of a Doppler profile including the effects of resonance scattering was performed in IG02; however, they used two simplifying assumptions that we relax here. The first assumption we relax is that of very optically thick resonance lines, and the second is that of a constant expansion velocity. It is also desirable to recast the results of IG02 in terms of the formalism of OC01 in order to facilitate comparison of results from different model parameters.

To include the effects of resonance scattering in the OC01 formalism, we multiply the integrand of Equation 8 of OC01 by the normalized escape probability $p(\mu)/\beta$, giving

$$L_x = \frac{C\dot{M}^2}{2v_\infty^2} \int_{R_*}^{\infty} dr H[w(r) - |x|] \frac{f(r)}{r^2 w^3(r)} \left\{ e^{-\tau_c(\mu,r)} \frac{p(\mu)}{\beta} \right\}_{\mu=-x/w(r)}. \tag{6}$$

Here

$$p(\mu) = \frac{1 - e^{-\tau_\mu}}{\tau_\mu} \tag{7}$$

is the angle-dependent Sobolev escape probability and

$$\beta = \frac{1}{2} \int_{-1}^{1} d\mu \, p(\mu) \tag{8}$$

is the angle-averaged Sobolev escape probability. The physical motivation for this term comes from the Sobolev theory developed in IG02; the escape probability $p(\mu)$ describes the angular distribution of escaping photons, while the factor β gives the increased emission over thermal resulting from the trapping of scattered photons. Another way to look at the factor β is that it normalizes the emission to be the same as for the case of no resonance scattering, which should be the case as long as photons are not trapped long enough to be thermalized.

In these equations,

$$\tau_\mu = \frac{\tau_0}{1 + \sigma\mu^2} \tag{9}$$

is the Sobolev optical depth, where

$$\sigma = \frac{r}{v}\frac{\partial v}{\partial r} - 1 = \frac{\beta_v u}{1 - u} - 1. \tag{10}$$

Here we have used the inverse radial coordinate $u \equiv R_*/r$; we have also used β_v to denote the exponent of the velocity law, $v(r) = v_\infty(1 - R_*/r)^{\beta_v}$, in order to avoid confusion with the angle-averaged Sobolev escape probability.

The factor τ_0 gives the Sobolev optical depth in the lateral direction $\mu = 0$; it is given by

$$\tau_0 = \frac{3}{8} \frac{\lambda}{r_e} \frac{c}{v} f_i \, n_i \, \sigma_T \, r. \tag{11}$$

Here r_e is the classical electron radius; σ_T is the Thomson cross-section; f_i is the oscillator strength of the transition; and n_i is the ion density. To explicitly put in all dependence on the radial coordinate, we use the continuity equation, $\dot{M} = 4\pi\rho r^2 v$, giving

$$\tau_0 = \frac{\lambda r_e c \dot{M}}{4 R_* v_\infty^2} \left(f_i \frac{n_i}{\rho} \right) \frac{u}{w^2(u)} = \tau_{0,*} \frac{u}{w^2(u)} \tag{12}$$

where we have defined the parameter

$$\tau_{0,*} = \frac{\lambda r_e c \dot{M}}{4 R_* v_\infty^2} \left(f_i \frac{n_i}{\rho} \right) \tag{13}$$

as a characteristic Sobolev optical depth. The factor

$$\frac{n_i}{\rho} = \frac{n_i}{n_e} \frac{n_e}{\rho} = \frac{A_i \, q_i \, f_X}{\mu_N \, m_p} \tag{14}$$

gives the ratio of the ion number density to the mass density. Here A_i is the abundance of the element relative to hydrogen; q_i is the ion fraction; f_X is the filling factor of X-ray emitting plasma; and $\mu_N m_p$ is the mean mass per particle. We take this ratio to be a constant with radius, although in principle the ion fraction and filling factor could vary.

In this paper, we take $\tau_{0,*}$ as a free parameter. τ_μ then has the radial and angular dependence given by Equations 9 and 12.

In order to evaluate β, it is necessary to perform the integral over μ. In the approximation that the Sobolev optical depth is very large, the integral is analytic, and we get

$$\frac{p(\mu)}{\beta} = \frac{1 + \sigma\mu^2}{1 + \sigma/3}. \tag{15}$$

If we cannot make this approximation, the integral over μ cannot be evaluated analytically. However, there is an analytic approximation given in Castor (2004, pp. 128-129, attributed to Rybicki) that is accurate to $\sim 1.5\%$. We use this approximation to calculate β for finite values of $\tau_{0,*}$.

IG02 assume a constant wind expansion velocity ($\beta_v = 0$) and that the Sobolev optical depth is large. Under these assumptions, we recover the expression $p(\mu)/\beta = (3/2)(1 - \mu^2)$, which has the same μ dependence as the result derived in IG02.

The approximation of constant expansion is not unreasonable at large radii, but $\beta_v = 1$ is closer to the actual velocity law of ζ Pup, and it is no more difficult to implement in our model. However, we wish to consider the possibility that the *effective* β_v for the purposes of resonance scattering could be different than for the wind as a whole. For example, since the X-ray emitting plasma is too ionized to have much effective line opacity in the UV, it should not be driven, and thus the local velocity gradient might be better described in terms of a $\beta_v = 0$ model without radial acceleration, even while the overall mean velocity of the wind is described well by a velocity law with $\beta_v = 1$.

Let us thus define $\beta_{\rm Sob}$ to be the value of β_v used in calculating σ. We consider two cases in this work: $\beta_{\rm Sob} = 0$ corresponds to no local velocity gradient for X-ray emitting plasma, and $\beta_{\rm Sob} = 1\,(= \beta_v)$ means that the local X-ray and global bulk wind velocity gradients are equal.

We have implemented this as a local model in XSPEC. The Sobolev optical depth has angular and radial dependence as given by Equations 9 and 12. The additional parameters added to the OC01 model are a switch to turn on or off completely optically thick scattering; the characteristic Sobolev optical depth $\tau_{0,*}$ (used when the completely optically thick switch is off); and the value of the velocity law exponent used in calculating σ, $\beta_{\rm Sob}$.

In Figures 3 and 4 we compare the effects of various values of $\tau_{0,*}$ and $\beta_{\rm Sob}$. The trend is for higher values of $\tau_{0,*}$ and lower values of $\beta_{\rm Sob}$ to give more symmetric profiles.

4.2. Best fit model including resonance scattering

In this section we fit He-like profile models including resonance scattering to the O VII and N VI complexes. We fit each complex twice: once assuming $\beta_{\rm Sob} = 1$ and once assuming $\beta_{\rm Sob} = 0$. The best-fit models are shown in Figures 5-8. The best fit parameters are given in Tables 2 and 3.

The O VII profile is well fit by either value of $\beta_{\rm Sob}$. We tested goodness of fit by comparing the fit statistic of 1000 Monte Carlo realizations of the model to the fit statistic of the data; both models are formally acceptable. The fit with $\beta_{\rm Sob} = 1$ is better than that with $\beta_{\rm Sob} = 0$, but only by $\Delta C = 3.8$, which is about 2σ for one interesting parameter. The fit with $\beta_{\rm Sob} = 0$ has a significantly smaller value of $\tau_{0,*}$ than the fit with $\beta_{\rm Sob} = 1$, as would be expected. The fit with $\beta_{\rm Sob} = 1$ is statistically consistent with the approximation that the Sobolev optical depth becomes infinite.

The N VI profile is much better fit by either model including resonance scattering than

it is by the original model. Furthermore, the model with $\beta_{\rm Sob} = 0$ gives a significantly better fit than the model with $\beta_{\rm Sob} = 1$. However, neither model is formally acceptable, and even the $\beta_{\rm Sob} = 0$ model shows residuals of the same qualitative form as the original model, albeit of a much lower strength. For both models including resonance scattering, the optically thick approximation gives a better fit than a profile with finite Sobolev optical depth.

To test the significance of profile broadening introduced by coadding data with random systematic errors in the wavelength scale, we have also fit each best-fit model with an additional 7 mÅ Gaussian broadening. In all cases, the best-fit parameters did not change significantly and the fit statistics were not significantly worse. Thus we conclude that our analysis is not strongly affected by this broadening.

5. Discussion

5.1. Comparison of results

The profile fits presented in § 3.2 clearly show that the O VII and N VI He-like triplet complexes in ζ Pup cannot be fit by models that assume the same profile shapes for the resonance and intercombination lines. The profile fits presented in § 4.2 show that these complexes can be much better fit by a model including the effects of resonance scattering.

However, although the O VII complex is well fit by a model including the effects of resonance scattering, the N VI complex shows differences in profile shape between the resonance and intercombination line that are greater than our model can reproduce, even under the most generous conditions ($\tau_{0,*} \rightarrow \infty, \beta_{\rm Sob} = 0$). Furthermore, one would expect the two complexes to show relatively similar parameters; for example, since the elemental abundance of nitrogen appears to be roughly twice that of oxygen, one would expect the parameter $\tau_{0,*}$ to be about twice as large for the fit to N VI as it is for O VII. But a fit to the N VI profile with $\beta_{\rm Sob} = 0$ and $\tau_{0,*} \approx 10$ (roughly twice the value measured for O VII) would give a substantially worse fit than a model with infinite Sobolev optical depth, which itself has significant residuals.

The fact that the apparent discrepancy between the shapes of the resonance and intercombination line profiles is much greater for N VI than for O VII implies that whatever the symmetrizing mechanism for the resonance line is, it is significantly stronger for N VI. There is no obvious explanation for this in the resonance scattering paradigm.

5.2. Plausibility of the importance of resonance scattering

It is worth revisiting the plausibility arguments of IG02 to confirm that one would expect resonance scattering to be important for these ions in the wind of ζ Pup. The relevant quantities to estimate are the Sobolev optical depth and the ratio of the Sobolev length to the cooling length.

The Sobolev length is given by

$$L_\mu = \frac{1+\sigma}{1+\sigma\mu^2}\frac{v_{\rm th}}{dv/dr} = \frac{v_{\rm th}}{v/r}\frac{1}{1+\sigma\mu^2} \tag{16}$$

(e.g. Gayley 1995). The cooling length is given by

$$\frac{5}{2}\frac{k\Delta T}{n_e\lambda}v, \tag{17}$$

as derived in IG02.

Taking the ratio,

$$\frac{L_c}{L_\mu} = \frac{5}{2}\frac{k\Delta T}{n_e\Lambda}\frac{v}{v_{th}}\frac{v}{r}(1+\sigma\mu^2) \tag{18}$$

$$= \frac{5}{2}\frac{k\Delta T}{\Lambda}\frac{4\pi\mu_N m_p}{\dot{M}}\frac{v_\infty}{v_{th}}v_\infty^2 R_*\frac{w^3(u)f_X}{u}(1+\sigma\mu^2) \tag{19}$$

where we have used $\dot{M} = 4\pi\mu_N m_p n_e r^2 v$ for a smooth wind, and added a filling factor f_X to correct for the ratio of the density of the X-ray emitting plasma to the mean density expected for a smooth wind.

Putting in some representative numbers appropriate to ζ Pup, we have

$$\frac{L_c}{L_\mu} = 10\,(1+\sigma\mu^2)\,\frac{w^3(u)f_X}{u}\,\frac{1}{\dot{M}_6} \tag{20}$$

where $\dot{M}_6$ is the mass-loss rate in units of $10^{-6}\,{\rm M}_\odot\,{\rm yr}^{-1}$. We have used $\Lambda = 6{\times}10^{23}\,{\rm erg\,s^{-1}\,cm^3}$, $\Delta T = 2{\rm MK}$, $\mu_N = 0.6$, $v_{th} = 50\,{\rm km\,s^{-1}}$, $v_\infty = 2500\,{\rm km\,s^{-1}}$, and $R_* = 1.4\times10^{12}\,{\rm cm}$.

This expression is greater than unity for lateral escape except at small radii ($r < 2R_*$) if the filling factor is of order unity. However, if the filling factor is significantly less than unity, the Sobolev approximation may not be valid.

We now consider the expected values of the characteristic Sobolev optical depth,

$$\tau_{0,*} = \frac{\lambda\, r_e\, c\, \dot{M}}{4R_*\, v_\infty^2}\left(f_i\frac{n_i}{\rho}\right) = \frac{\lambda\, r_e\, c\, \dot{M}}{4\mu_N\, m_p\, R_*\, v_\infty^2} f_i\, A_i\, q_i\, f_X. \tag{21}$$

Putting in appropriate values, we get

$$\tau_{0,*} = 120 \left(f_i \frac{A_i}{10^{-3}} \frac{\lambda}{20\,\text{Å}} \right) q_i \, f_X \, \dot{M}_6 \tag{22}$$

We give calculations of $\tau_{0,*}/q_i f_X$ for important lines in O star spectra in Table 4. We have assumed solar abundances for all elements except C, N, and O (Anders & Grevesse 1989). We assumed that the sum of CNO is equal to the solar value, with carbon being negligible and with nitrogen having twice the abundance of oxygen; this is an estimate based on the observed X-ray emission line strengths. Note that the Sobolev optical depth scales with the wavelength of the transition; this means that the Sobolev optical depths are significantly smaller for an X-ray transition than they are for a comparable UV transition.

Again, if the X-ray filling factors are of order unity, the characteristic Sobolev optical depths for the resonance lines of N VI and O VII are large, but X-ray filling factors of order 10^{-3} or less are sufficient to cause the lines to become optically thin. However, the requirement that the Sobolev length in the lateral direction be smaller than the cooling length is about as stringent, so that if resonance scattering is important for strong lines, the Sobolev approximation should also be valid.

The high filling factors required are at odds with the simple two-component fluid picture of the OC01 model, since the X-ray filling factors are known to be very low. However, if we take the wind to be resolved on scales of order the Sobolev length into the two components, the filling factor would just be ratio of the local density to the mean density at that radius. This filling factor would still likely be less than unity for the X-ray emitting plasma, but not as low as the X-ray filling factor for the whole wind. This conjecture is a significantly stronger assumption than is made in OC01.

5.3. Impact of resonance scattering on Doppler profile model parameters

If resonance scattering is important in Doppler profile formation in the X-ray spectra of O stars, it may lead to a partial reconciliation with the literature mass-loss rates. The best fit models for O VII have $\tau_* = 4.1$, and the best fit model for N VI has $\tau_* = 3.0$. If we speculate that somehow the resonance line of N VI is even further symmetrized than predicted by our model, as the residuals in our best-fit model imply, the value of τ_* demanded by the intercombination line profile residuals should be somewhat higher; a reasonable guess would be $\tau_* \sim 4 - 5$.

These characteristic optical depths are higher than those measured by Kramer et al. (2003) for ζ Pup by applying the model of OC01 to Doppler profiles observed with the

Chandra HETGS; the lines studied in that paper were mostly resonance lines as well. They are still somewhat lower than one would expect given the literature mass-loss rates; however, a detailed comparison with opacity calculations and mass-loss rates remains to be done. New, sophisticated analyses of UV absorption line profiles indicate that the published mass-loss rates of O-star winds are too high (Massa et al. 2003; Hillier et al. 2003; Bouret et al. 2005); the most recent systematic analysis of galactic O stars finds that for at least some spectral types, the published mass-loss rates must be at least an order of magnitude too great (Fullerton et al. 2006). This leads to the curious possibility that measurements of the mass-loss rates of O stars using Doppler profiles of X-ray emission lines could be *higher* than the most recent UV line profile measurements, which is the opposite of the problem currently being addressed by the community.

Our measurements provide suggestive constraints on the radial dependence of the X-ray emission. The O VII fit has $q \sim 0$, and the onset radius for X-ray emission is not well constrained apart from being significantly inside the radius of optical depth unity. Although our model does not provide a good fit to N VI, a model that accounts for the symmetrization of the resonance line may also show a similar radial distribution of X-ray emitting plasma. If the characteristic optical depths to X-rays are of order a few at longer wavelengths in the wind of ζ Pup, these constraints on the radial dependence may help to break possible profile fitting degeneracies. A profile model with $q \equiv 0$ and u_0 obscured by absorption would have two fitting parameters for optically thick lines (τ_* and $\tau_{0,*}$) and one for optically thin lines (τ_*). Thus, high signal-to-noise, optically thin Doppler profiles with significant continuum absorption may provide robust measurements of the mass-loss rates of O stars. A good candidate for this is the 16.78 Å line of Fe XVII, which is likely not to be optically thick, and which is not blended with other lines.

5.4. Future work

Here we give a list of questions raised by this analysis that should be addressed in future work.

1. The discrepancies in the fits in this paper must be resolved. The fact that we cannot fit the N VI profile well is unsatisfactory. The difference between the appearance of the N VI complex and the O VII complex requires explanation.

2. The effect of resonance scattering on other resonance lines in the X-ray spectrum should be considered. Furthermore, unless we can make concrete predictions for the importance of resonance scattering for these lines, there may be significant fitting degeneracies

between resonance scattering and low characteristic continuum optical depths.

3. The effect of multiple lines on resonance scattering should be explored. Of special importance is the calculation of the profile of a close doublet, such as Lyman α. In that case, the splitting between the two lines is of order the thermal velocity of the ions.

6. Conclusions

We have fit Doppler profile models based on the parametrized model of OC01 to the He-like triplet complexes of O VII and N VI in the high signal-to-noise XMM-*Newton* RGS X-ray spectrum of ζ Pup. We find that the complexes cannot be well fit by models assuming the same shape for the resonance and intercombination lines; the predicted resonance lines are too blue and the predicted resonance lines are too red. This effect is what is predicted qualitatively if resonance scattering is important.

We find that models including the effects of resonance scattering give significantly better fits. However, there is significant disagreement between the O VII and N VI profiles in the degree of resonance line symmetrization that is difficult to understand in the framework of the resonance scattering model. Nevertheless, the general trend of the resonance scattering model to give more symmetrized profiles provides an interesting alternative (or supplement) to models that assume reduced wind attenuation due to reduced mass-loss rates and/or porosity.

We acknowledge useful conversations with David Cohen. We thank David Cohen and Dave Spiegel for their careful reading of the manuscript. MAL acknowledges NASA grant NNG04GL76G.

REFERENCES

Anders, E. & Grevesse, N. 1989, Geochim. Cosmochim. Acta, 53, 197

Bouret, J.-C., Lanz, T., & Hillier, D. J. 2005, A&A, 438, 301

Cash, W. 1979, ApJ, 228, 939

Cassinelli, J. P., Miller, N. A., Waldron, W. L., MacFarlane, J. J., & Cohen, D. H. 2001, ApJ, 554, L55

Cassinelli, J. P. & Swank, J. H. 1983, ApJ, 271, 681

Castor, J. I. 2004, Radiation Hydrodynamics (Radiation Hydrodynamics, by John I. Castor, pp. 368. ISBN 0521833094. Cambridge, UK: Cambridge University Press, November 2004.)

Cohen, D. H., de Messières, G. E., MacFarlane, J. J., Miller, N. A., Cassinelli, J. P., Owocki, S. P., & Liedahl, D. A. 2003, ApJ, 586, 495

Cohen, D. H., Leutenegger, M. A., Grizzard, K. T., Reed, C. L., Kramer, R. H., & Owocki, S. P. 2006, MNRAS, 368, 1905

Cooper, R. G. 1994, Ph.D. Thesis

Corcoran, M. F., Swank, J. H., Serlemitsos, P. J., Boldt, E., Petre, R., Marshall, F. E., Jahoda, K., Mushotzky, R., Szymkowiak, A., Arnaud, K., Smale, A. P., Weaver, K., & Holt, S. S. 1993, ApJ, 412, 792

Corcoran, M. F., Waldron, W. L., Macfarlane, J. J., Chen, W., Pollock, A. M. T., Torii, K., Kitamoto, S., Miura, N., Egoshi, M., & Ohno, Y. 1994, ApJ, 436, L95

den Herder, J. W., Brinkman, A. C., Kahn, S. M., Branduardi-Raymont, G., Thomsen, K., Aarts, H., Audard, M., Bixler, J. V., den Boggende, A. J., Cottam, J., Decker, T., Dubbeldam, L., Erd, C., Goulooze, H., Güdel, M., Guttridge, P., Hailey, C. J., Janabi, K. A., Kaastra, J. S., de Korte, P. A. J., van Leeuwen, B. J., Mauche, C., McCalden, A. J., Mewe, R., Naber, A., Paerels, F. B., Peterson, J. R., Rasmussen, A. P., Rees, K., Sakelliou, I., Sako, M., Spodek, J., Stern, M., Tamura, T., Tandy, J., de Vries, C. P., Welch, S., & Zehnder, A. 2001, A&A, 365, L7

Dere, K. P., Landi, E., Mason, H. E., Monsignori Fossi, B. C., & Young, P. R. 1997, A&AS, 125, 149

Donati, J.-F., Babel, J., Harries, T. J., Howarth, I. D., Petit, P., & Semel, M. 2002, MNRAS, 333, 55

Donati, J.-F., Howarth, I. D., Jardine, M. M., Petit, P., Catala, C., Landstreet, J. D., Bouret, J.-C., Alecian, E., Barnes, J. R., Forveille, T., Paletou, F., & Manset, N. 2006, MNRAS, 370, 629

Feldmeier, A., Oskinova, L., & Hamann, W.-R. 2003, A&A, 403, 217

Feldmeier, A., Puls, J., & Pauldrach, A. W. A. 1997, A&A, 322, 878

Fullerton, A. W., Massa, D. L., & Prinja, R. K. 2006, ApJ, 637, 1025

Gagné, M., Oksala, M. E., Cohen, D. H., Tonnesen, S. K., ud-Doula, A., Owocki, S. P., Townsend, R. H. D., & MacFarlane, J. J. 2005, ApJ, 628, 986

Gayley, K. G. 1995, ApJ, 454, 410

Hillier, D. J., Kudritzki, R. P., Pauldrach, A. W., Baade, D., Cassinelli, J. P., Puls, J., & Schmitt, J. H. M. M. 1993, A&A, 276, 117

Hillier, D. J., Lanz, T., Heap, S. R., Hubeny, I., Smith, L. J., Evans, C. J., Lennon, D. J., & Bouret, J. C. 2003, ApJ, 588, 1039

Ignace, R. & Gayley, K. G. 2002, ApJ, 568, 954

Kahn, S. M., Leutenegger, M. A., Cottam, J., Rauw, G., Vreux, J.-M., den Boggende, A. J. F., Mewe, R., & Güdel, M. 2001, A&A, 365, L312

Kramer, R. H., Cohen, D. H., & Owocki, S. P. 2003, ApJ, 592, 532

Landi, E., Del Zanna, G., Young, P. R., Dere, K. P., Mason, H. E., & Landini, M. 2006, ApJS, 162, 261

Lanz, T. & Hubeny, I. 2003, ApJS, 146, 417

Leutenegger, M. A., Paerels, F. B. S., Kahn, S. M., & Cohen, D. H. 2006, ApJ, in press

Lucy, L. B. & White, R. L. 1980, ApJ, 241, 300

Massa, D., Fullerton, A. W., Sonneborn, G., & Hutchings, J. B. 2003, ApJ, 586, 996

Miller, N. A., Cassinelli, J. P., Waldron, W. L., MacFarlane, J. J., & Cohen, D. H. 2002, ApJ, 577, 951

Oskinova, L. M., Feldmeier, A., & Hamann, W.-R. 2004, A&A, 422, 675

—. 2006, MNRAS, submitted

Owocki, S. P., Castor, J. I., & Rybicki, G. B. 1988, ApJ, 335, 914

Owocki, S. P. & Cohen, D. H. 2001, ApJ, 559, 1108

—. 2006, ApJ, in press

Porquet, D., Mewe, R., Dubau, J., Raassen, A. J. J., & Kaastra, J. S. 2001, A&A, 376, 1113

Waldron, W. L. & Cassinelli, J. P. 2001, ApJ, 548, L45

Waldron, W. L., Cassinelli, J. P., Miller, N. A., MacFarlane, J. J., & Reiter, J. C. 2004, ApJ, 616, 542

Table 1. List of observations with net exposure times

obsid [a]	$t_{\rm exp,R1}$ [b]	$t_{\rm exp,R2}$ [b]
0095810301	30.6	29.8
0095810401	39.7	38.3
0157160401	41.5	40.2
0157160501	32.8	32.8
0157160901	43.4	43.4
0157161101	27.0	27.0
0159360101	59.2	59.2
0159360301	22.0	22.0
0159360501	31.5	31.5
0159360901	46.6	46.6
0159361101	41.1	41.0

[a]XMM Observation ID.

[b]Net exposure time in ks.

Table 2. Model fit parameters for O VII

$\beta_{\rm Sob}$	q	τ_*	u_0	$\tau_{0,*}$	G [a]	n [b]	C [c]	MC [d]
$\cdots$	-0.21	1.6	0.62	$\cdots$	0.91	6.91	152.2	$\cdots$
1	$0.15^{+0.06}_{-0.07}$	$4.1^{+0.3}_{-0.4}$	> 0.68	> 50	$1.11^{+0.03}_{-0.04}$	6.88 ± 0.07	85.3	0.578
0	$0.15^{+0.07}_{-0.07}$	4.1 ± 0.4	> 0.63	$5.9^{+3.2}_{-1.8}$	$1.02^{+0.04}_{-0.03}$	6.88 ± 0.07	89.1	0.730

[a] $G = (f + i)/r$ is assumed not to vary with radius.

[b] Normalization of entire complex $(r + i + f)$ in units of 10^{-4} photons cm^{-2} s^{-1}.

[c] For 83 bins.

[d] Fraction of 1000 Monte Carlo realizations of model having C less than the data.

Note. — The first row gives the best fit for a model not including resonance scattering (i.e. the model of OC01 and Leutenegger et al.). The second row gives the best fit for a model including resonance scattering with $\beta_{\rm Sob} = 1$, and the last row has $\beta_{\rm Sob} = 0$. We used a value of $P = 1.67 \times 10^4$ for all O VII profile models (Leutenegger et al. 2006).

Table 3. Model fit parameters for N VI

$\beta_{\rm Sob}$	q	τ_*	u_0	$\tau_{0,*}$	G [a]	n [b]	n_β [c]	C [d]
$\cdots$	-0.34	0.5	0.58	$\cdots$	0.87	1.562	0	510.5
1	-0.09	2.1	0.50	thick	1.10	1.559	0.87	292.2
0	0.06	3.0	0.48	thick	1.15	1.552	1.25	188.4

[a] $G = (f + i)/r$ is assumed not to vary with radius.

[b] Normalization of entire N VI complex in units of 10^{-3} photons cm^{-2} s^{-1}.

[c] Normalization of C VI Lyman β in units of 10^{-5} photons cm^{-2} s^{-1}.

[d] For 117 bins.

Note. — The first row gives the best fit for a model not including resonance scattering (i.e. the model of OC01 and Leutenegger et al.). The second row gives the best fit for a model including resonance scattering with $\beta_{\rm Sob} = 1$, and the last row has $\beta_{\rm Sob} = 0$. The C VI Lyman β line is assumed to have the same values of q, τ_*, and u_0 as the N VI triplet, and is assumed not to be affected by resonance scattering. We used a value of $P = 1.01 \times 10^5$ for all N VI profile models (Leutenegger et al. 2006).

Table 4. Expected characteristic Sobolev optical depth

		λ [a]	f_i [b]	A_i [c]	$\tau_{0,*}/q_i\, f_X$ [d]
N VI	r	28.78	0.6599	0.9	103
	β	24.90	0.1478		20
N VII	Ly α	24.78	0.1387, 0.2775 [e]		19, 37
O VII	r	21.60	0.6798	0.45	40
	β	18.63	0.1461		7
O VIII	Ly α	18.97	0.1387, 0.2775 [e]		7, 14
Fe XVII		15.01	2.517	0.047	11
		15.26	0.5970		2.5
		16.78	0.1064		0.5
		17.05	0.1229		0.6
Ne IX	r	13.45	0.7210	0.12	7.0
	β	11.55	0.1490		1.2
Ne X	Ly α	12.13	0.1382, 0.2761 [e]		1.2, 2.4
Mg XI	r	9.17	0.7450	0.038	1.6
Mg XII	Ly α	8.42	0.1386, 0.2776 [e]		0.27, 0.53
Si XIII	r	6.65	0.7422	0.036	1.1
Si XIV	Ly α	6.18	0.1386, 0.2776 [e]		0.19, 0.37

[a]Wavelength in Å.

[b]Oscillator strengths are from CHIANTI (Dere et al. 1997; Landi et al. 2006).

[c]Assumed abundance relative to hydrogen in units of 10^{-3}.

[d]This number is calculated using Equation 22 assuming a mass-loss rate of $10^{-6}\,\mathrm{M}_\odot\,\mathrm{yr}^{-1}$.

[e] Lyman α is a doublet.

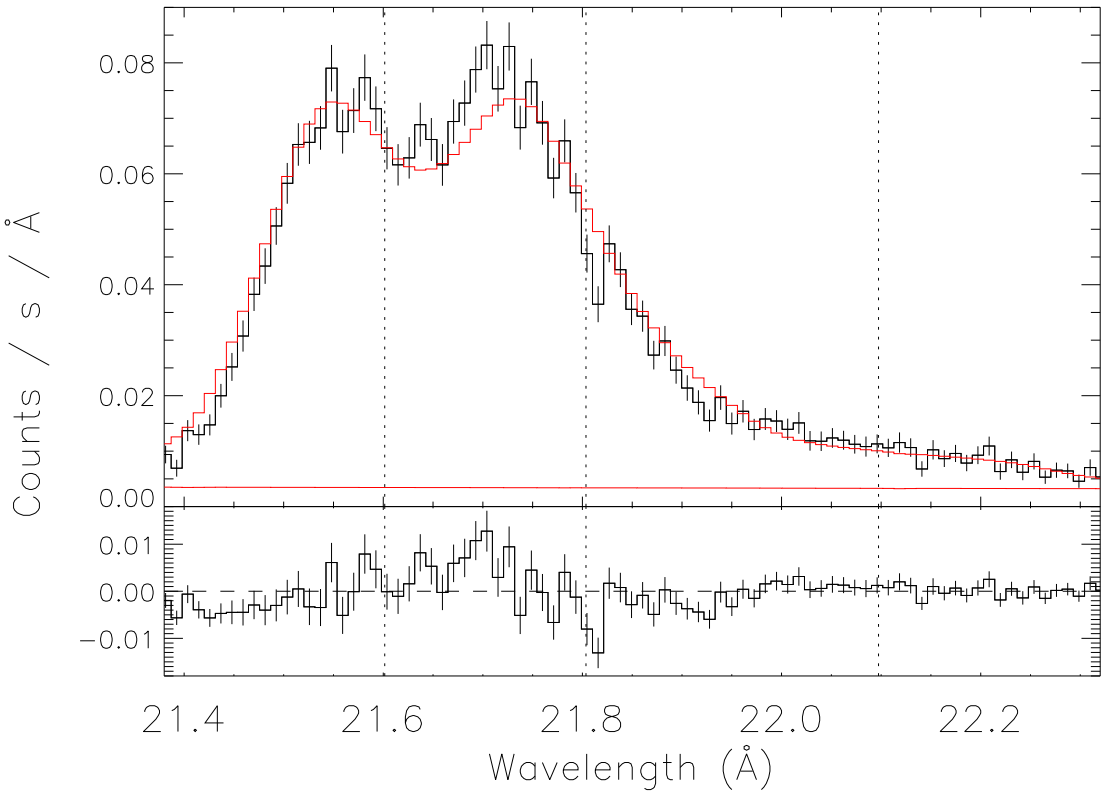

Fig. 1.— O VII triplet with best fit OC01 He-like triplet model (not including the effects of resonance scattering). The top panel shows the data in black with error bars and the model in red. The flat red line shows the assumed continuum strength. The bottom panel shows the fit residuals.

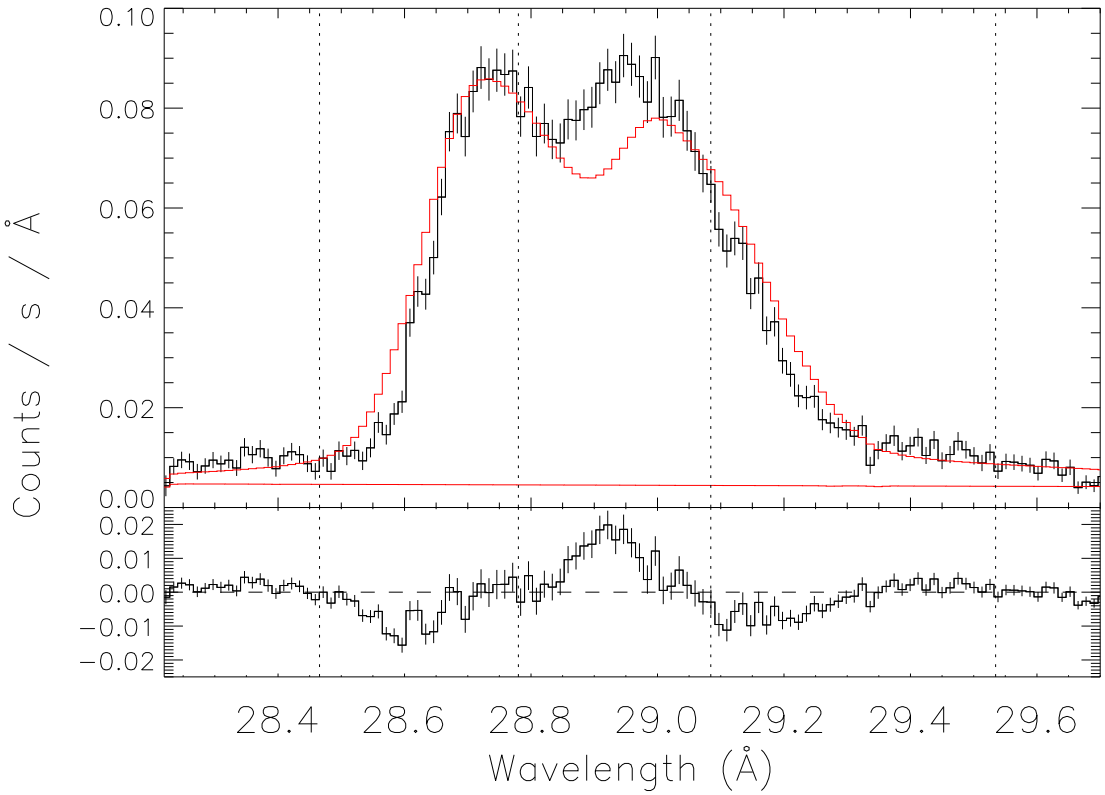

Fig. 2.— N VI triplet with best fit OC01 He-like triplet model (not including the effects of resonance scattering). Scheme is as in Figure 1. The C VI Lyman α line at 28.4656 Å is also included in the fit, as well as the other fits to the N VI triplet.

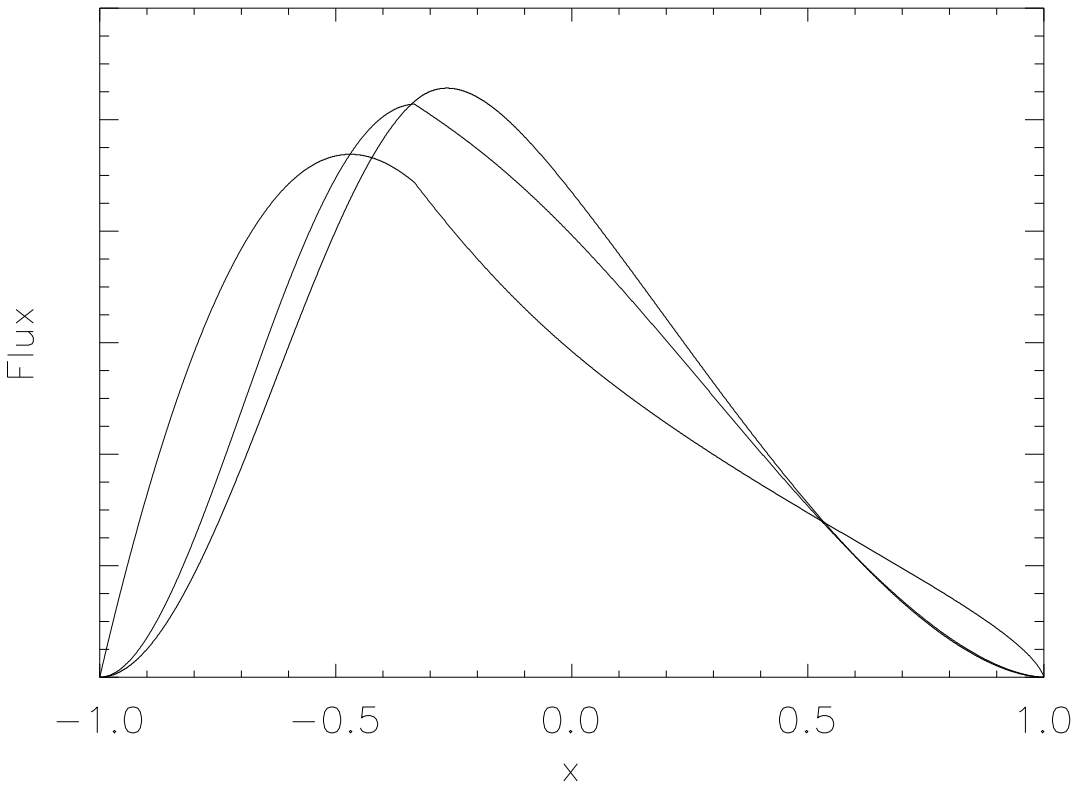

Fig. 3.— Comparison of the influence of different values of $\beta_{\rm Sob}$ on Doppler profile shape. All models have $q = 0$, $u_0 = 2/3$, and $\tau_* = 5$. The most asymmetric model is optically thin. Both of the other models use the approximation that $\tau_{0,*}$ is infinite; the more asymmetric of the two has $\beta_{\rm Sob} = 1$, while the least asymmetric has $\beta_{\rm Sob} = 0$.

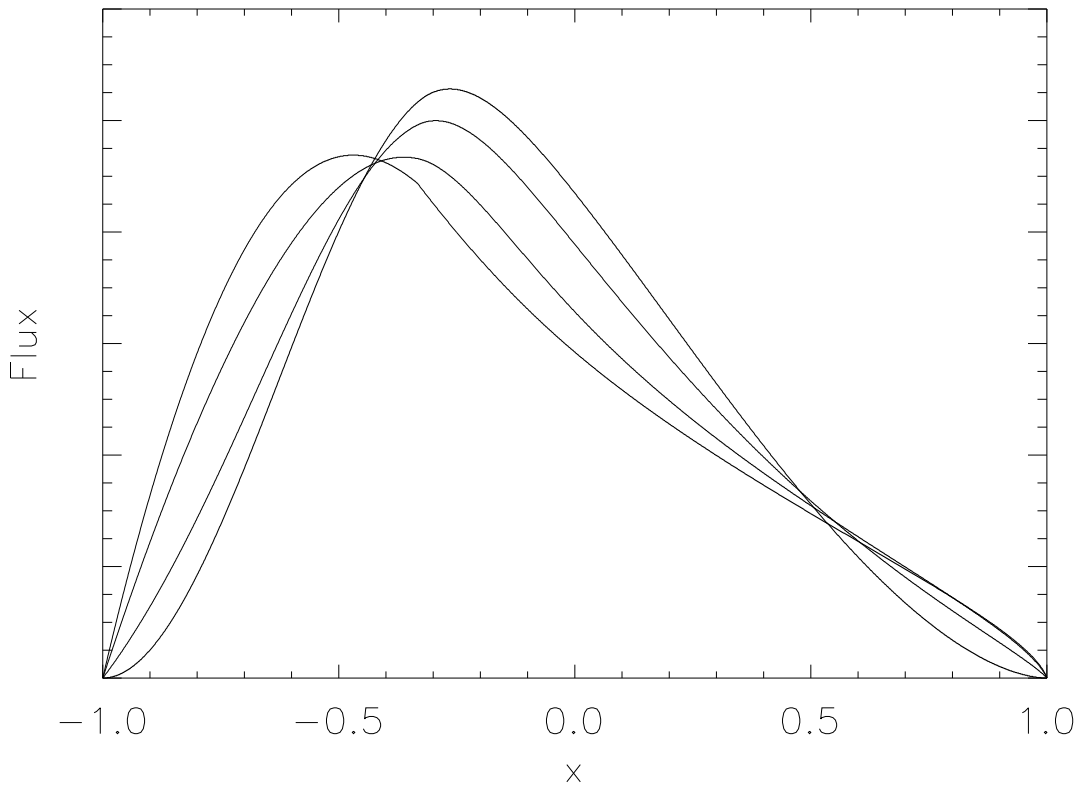

Fig. 4.— Comparison of the influence of various values of the characteristic Sobolev optical depth $\tau_{0,*}$ on Doppler profile shape. All models have $q = 0$, $u_0 = 2/3$, $\tau_* = 5$, and $\beta_{\rm Sob} = 0$. In order from most asymmetric to least the models have $\tau_{0,*} = 0, 1, 10, \infty$.

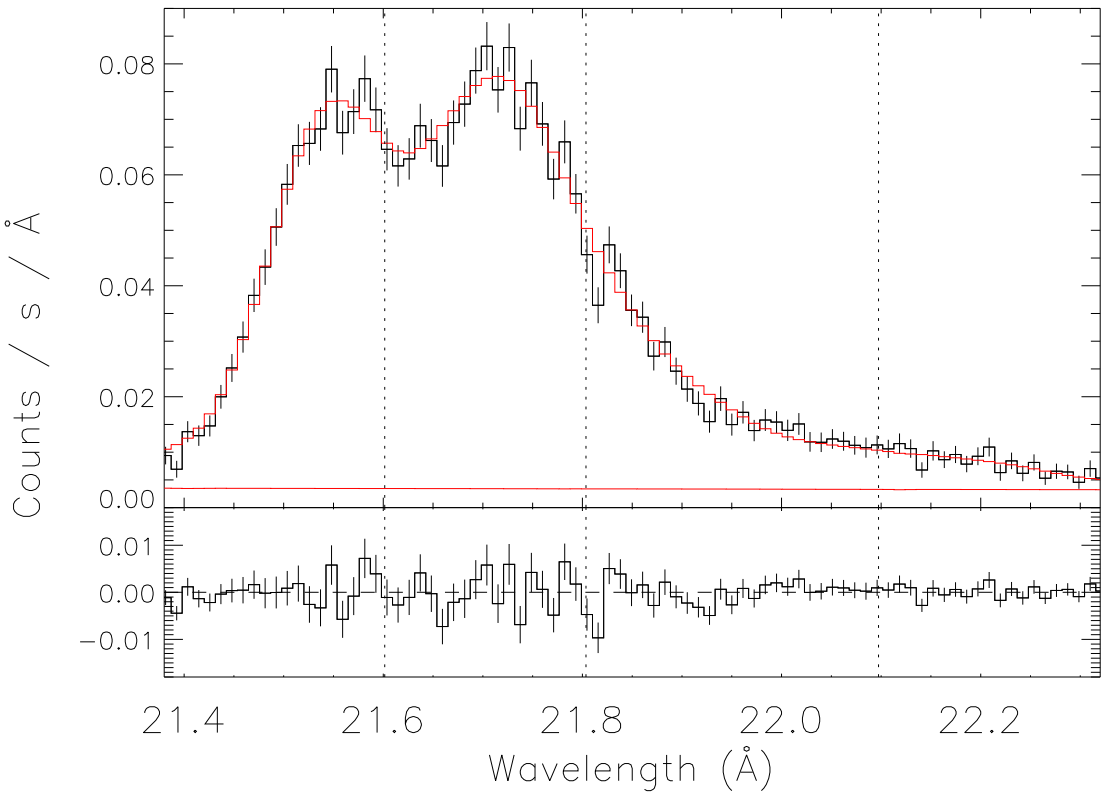

Fig. 5.— O VII triplet with best fit model assuming resonance scattering with $\beta_{\rm Sob} = 1$. Scheme is as in Figure 1.

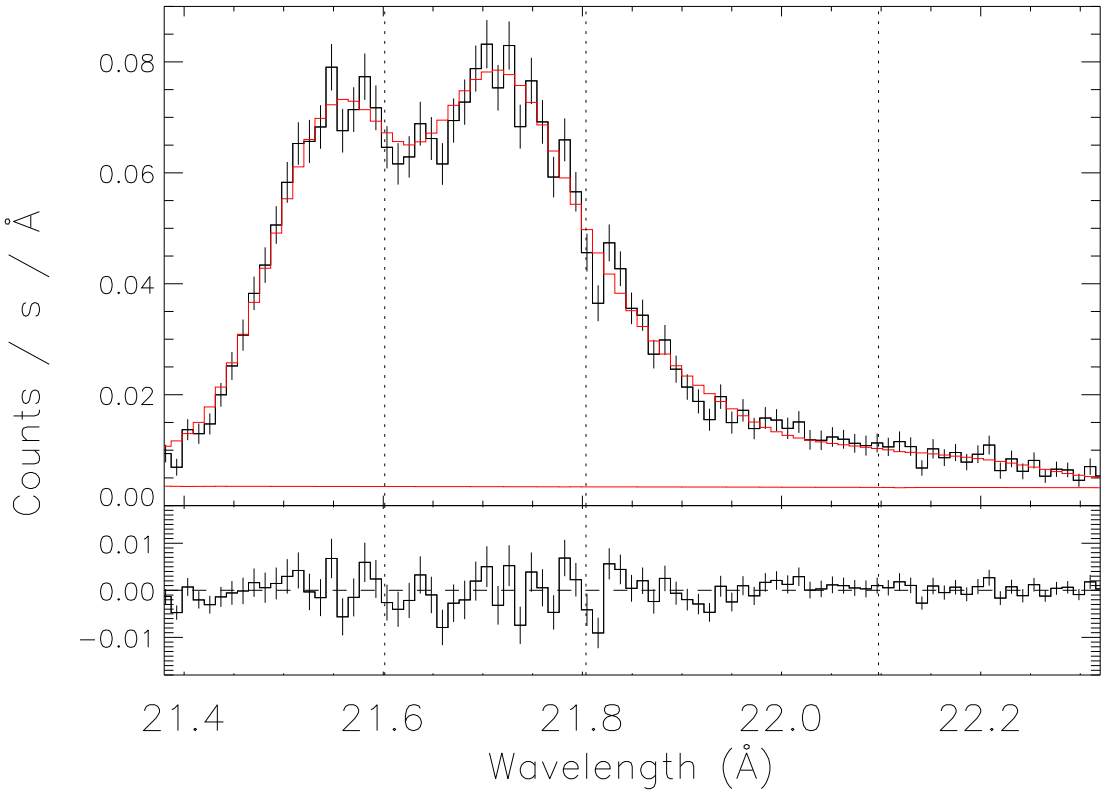

Fig. 6.— O VII triplet with best fit model assuming resonance scattering with $\beta_{\rm Sob} = 0$. Scheme is as in Figure 1.

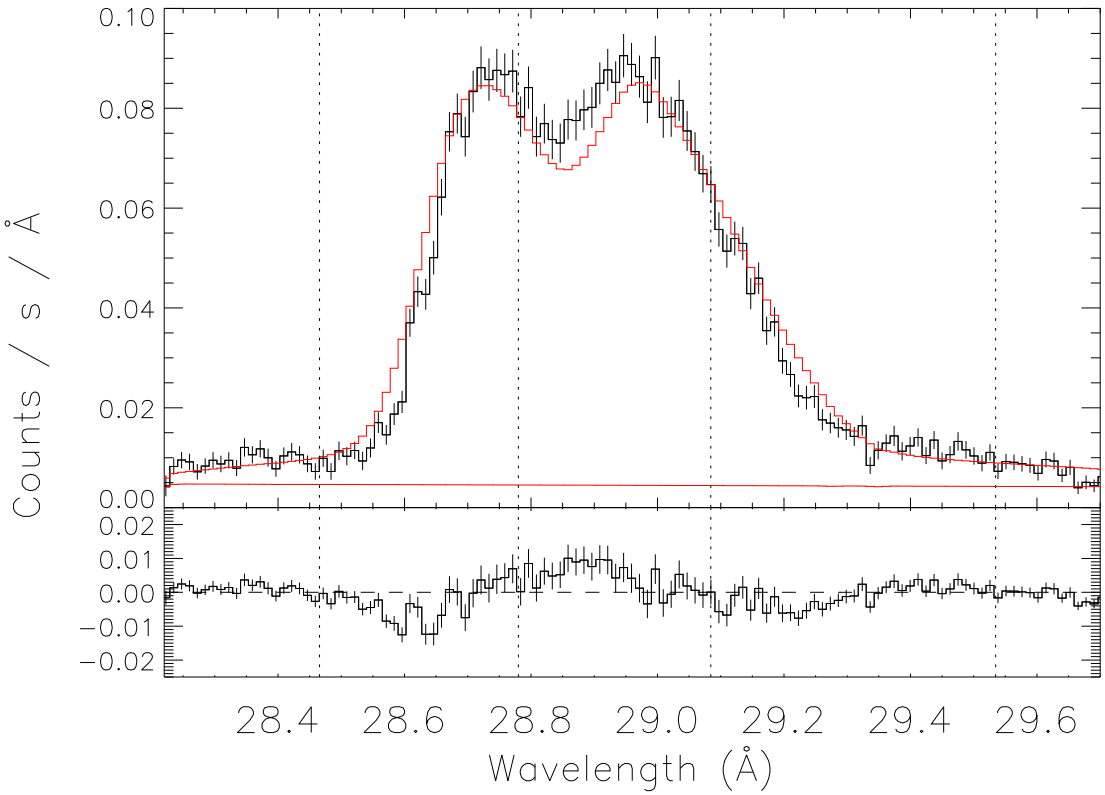

Fig. 7.— N VI triplet with best fit model assuming resonance scattering with $\beta_{\rm Sob} = 1$. Scheme is as in Figure 1.

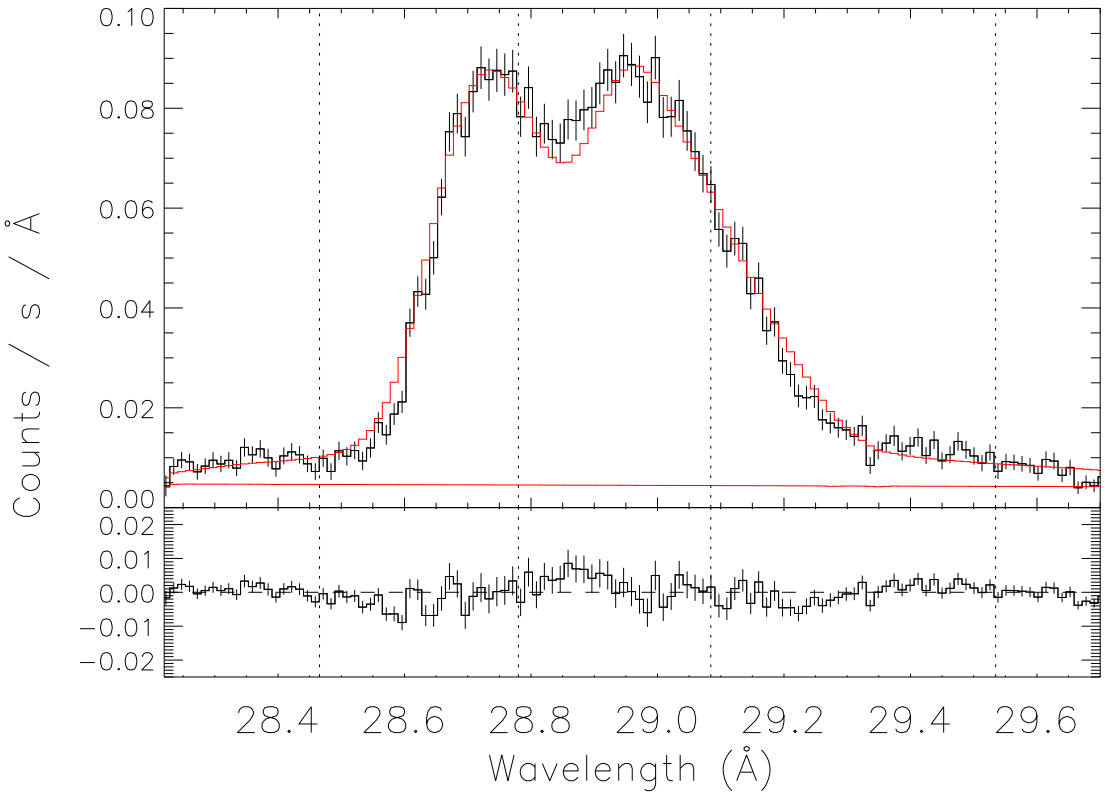

Fig. 8.— N VI triplet with best fit model assuming resonance scattering with $\beta_{\rm Sob} = 0$. Scheme is as in Figure 1.